PHYSICAL REVIEW B **81**, 064401 (2010)

Determination of the magnetic structure of Yb_3Pt_4: $k=0$ local-moment antiferromagnet

Y. Janssen,[1,*] M. S. Kim,[1] K. S. Park,[1,2] L. S. Wu,[2] C. Marques,[2] M. C. Bennett,[2] Y. Chen,[3,4] J. Li,[3,4] Q. Huang,[3]
J. W. Lynn,[3] and M. C. Aronson[1,2]
[1]*Condensed Matter Physics and Materials Science Department, Brookhaven National Laboratory, Upton, New York 11973, USA*
[2]*Department of Physics and Astronomy, Stony Brook University, Stony Brook, New York 11794, USA*
[3]*NIST Center for Neutron Research, NIST, Gaithersburg, Maryland 20899, USA*
[4]*Department of Materials Science, University of Maryland, College Park, Maryland 20742, USA*
(Received 26 June 2009; revised manuscript received 8 December 2009; published 1 February 2010)

We have used neutron-diffraction measurements to study the zero-field magnetic structure of the intermetallic compound Yb_3Pt_4, which was earlier found to order antiferromagnetically at the Néel temperature $T_N=2.4$ K, and displays a field-driven quantum-critical point at 1.6 T. In Yb_3Pt_4, the Yb moments sit on a single low-symmetry site in the rhombohedral lattice with space group $R\bar{3}$. The Yb ions form octahedra with edges that are twisted with respect to the hexagonal unit cell, a twisting that results in every Yb ion having exactly one Yb nearest neighbor. Below T_N, we found new diffracted intensity due to a $\boldsymbol{k}=0$ magnetic structure. This magnetic structure was compared to all symmetry-allowed magnetic structures and was subsequently refined. The best-fitting magnetic-structure model is antiferromagnetic and involves pairs of Yb nearest neighbors on which the moments point almost exactly toward each other. This structure has moment components within the *ab* plane as well as parallel to the *c* axis although the easy magnetization direction lies in the *ab* plane. Our magnetization results suggest that besides the crystal-electric-field anisotropy, anisotropic exchange favoring alignment along the *c* axis is responsible for the overall direction of the ordered moments. The magnitude of the ordered Yb moments in Yb_3Pt_4 is $0.81\mu_B/\text{Yb}$ at 1.4 K. The analysis of the bulk properties, the size of the ordered moment, and the observation of well-defined crystal-field levels argue that the Yb moments are spatially localized in zero field.

DOI: 10.1103/PhysRevB.81.064401 PACS number(s): 75.25.−j, 71.27.+a, 75.20.Hr

I. INTRODUCTION

The quantum-critical state in stoichiometric Yb intermetallic compounds is often associated with anomalous metallic states, non-Fermi-liquid behavior,[1–4] and, most recently, with heavy-Fermion superconductivity.[5] Some stoichiometric Yb antiferromagnets show field-induced quantum-critical points (QCP) and can thus be tuned toward quantum criticality by applying a magnetic field.[2,3] Different scenarios[4] can be related to antiferromagnetic (AF) QCPs either involving large localized-moment order or involving small-moment spin-density wavelike order. We have recently[6,7] identified the binary intermetallic compound Yb_3Pt_4 as a stoichiometric Yb-based compound with a field-induced QCP.

We have characterized Yb_3Pt_4 by measuring thermodynamic and transport properties.[6,7] The magnetic susceptibility χ of Yb_3Pt_4 above 200 K is well described by a Curie-Weiss expression involving the full Yb^{3+} moment of $4.5\mu_B$. Yb_3Pt_4 orders antiferromagnetically at the Néel temperature $T_N=2.4$ K, releasing $\sim 0.8R \ln 2$ of entropy, consistent with largely localized Yb moments. Since the local symmetry of the Yb ions is triclinic, the manifold of crystal-field split states consists of four doublets. This scenario was confirmed in measurements of the specific heat C, which found that the ground doublet is well separated from the first excited doublet. The resistivity below T_N is quadratic in temperature, the susceptibility χ weakly temperature dependent, and the Sommerfeld constant $\gamma=C/T$ vanishingly small. We concluded that the ordered state is a Fermi liquid, most likely weakly coupled to the ordered Yb moments. These experimental data indicate that the f electrons are likely localized on the Yb ions and are thus excluded from the Fermi surface. Besides this zero-field behavior, we have also shown that a field-induced quantum-critical point can be reached by applying fields of ~ 1.6 T and that the low-temperature high-field state is also a Fermi liquid.

Some physical parameters important to understanding the properties of Yb_3Pt_4 cannot be directly obtained from thermodynamic measurements but need to be determined by scattering methods. The magnetic propagation vector, which describes whether the magnetic structure is commensurate or incommensurate with the crystal lattice, is important for the underlying magnetic fluctuations and their coupling to quasiparticles. The order parameter, i.e., the temperature dependence of the ordered magnetic moment, can show whether the ordering transition is continuous or discontinuous. The magnitude and direction of the ordered Yb moments, needed to rationalize the ordered-moment scenario (localized or itinerant), is determined by the magnetic structure. We have used neutron-diffraction experiments to determine all these and the results are described in this paper. Note that although the magnetism of related R_3Pt_4 (R=rare-earth element) compounds has been investigated[8,9] and the R=Ce compound was found to be a local-moment system, there are no magnetic-structure data available for comparison. The magnetic structure of isostructural Yb_3Pd_4 was reported as a complex $\boldsymbol{k}=0$ structure.[10]

This paper is organized as follows. We will give a description of the Yb_3Pt_4 crystal structure that provides the groundwork for understanding the magnetically ordered structure. Then we will give results of neutron-diffraction experiments and provide symmetry-allowed magnetic-structure models obtained by representation analysis. We will give our best-fitting magnetic-structure model. Finally, with the aid of specific-heat, inelastic neutron scattering and single-crystal magnetization data, we discuss the ordered Yb 4*f* moments in terms of a local-moment picture.

II. EXPERIMENTS

Small (up to ~3 mg) single crystals of Yb_3Pt_4 were grown out of a high-temperature ternary solution,[11–13] rich in Pb.[7] A polycrystalline sample of Yb_3Pt_4 was made by combining the yields of 12 different growths. For initial characterization, we used a Philips diffractomer employing Cu $K\alpha$ radiation to measure a powder x-ray diffraction pattern of finely ground crystals taken from each growth. The diffraction patterns were analyzed with the program Rietica,[14] using a Le Bail-type[15] of refinement. As we will show below, they can be indexed according to the space group $R\bar{3}$, with average lattice parameters $a=12.94(1)$ Å and $c=5.655(5)$ Å. These results are consistent with values $a=12.888$ Å and $c=5.629$ Å which were reported previously.[16] No reflections from impurity phases were detected in any of the batches used to make the neutron-diffraction sample, which amounted to about 7 g. We note that we have measured the specific heat, ac susceptibility, and dc magnetization on crystals taken from many different growths and in no case have we found a detectable difference in Neel temperature or moment. Additionally, we prepared a single crystal of about 60 mg and used it for a single-crystal neutron-diffraction experiment.

Neutron-powder-diffraction data were collected using the high-resolution neutron-powder diffractometer BT-1 and the high-flux double-focusing triple-axis spectrometer BT-7 at the NIST Center for Neutron Research NCNR. Samples were loaded in a V (Al) can for the BT-1 (BT-7) experiment. In both experiments, an ILL "orange" cryostat was used, for full-pattern base-temperature measurements at ~1.4 K, and for a full-pattern measurement at 5.1 K (5 K) in the BT-1 (BT-7) experiment. A Ge 311 (PG 002) monochromator produced neutrons with a wavelength $\lambda=2.079$ Å (2.359 Å) and data were collected over the angular range of $2\theta=3-168°$ (5–60°) with a step size of 0.05° (0.1°) in the BT-1 (BT-7) experiment. Additionally, the 60-mg single crystal of Yb_3Pt_4 was aligned such that a (110) reflection was in the Bragg condition and was subsequently used for a single-crystal neutron-diffraction experiment conducted between 1.4 and 4 K on the triple-axis instrument BT-9 at NCNR-NIST. The neutron-diffraction data were analyzed by the Rietveld method using the FULLPROF computer program suite.[17] Representation analysis to determine possible magnetic structures was performed using the computer program SARAH.[18] The size of the ordered moments were calculated from the refinement results using the program FULLPROF studio.[17,19]

Inelastic neutron-scattering experiments were performed on the same 7-g powder sample in the BT-7 double-focusing triple-axis spectrometer with a fixed final energy of 14.7 meV, and at several fixed wave vectors and several different temperatures both above and below T_N. We used a double-focusing PG monochromator and a horizontally focusing analyzer to obtain maximum intensity.

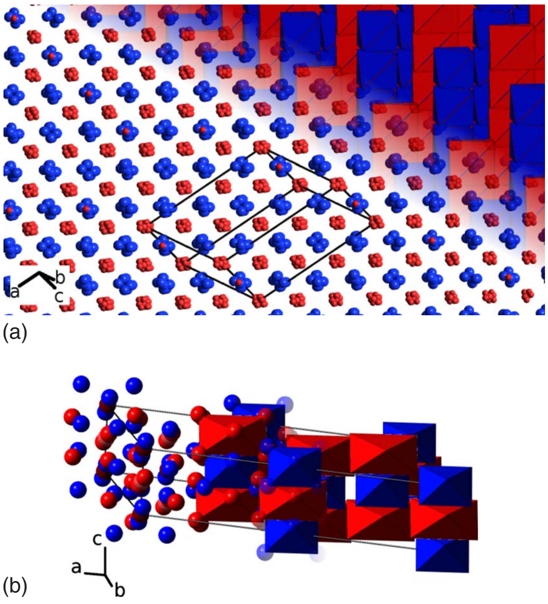

FIG. 1. (Color online) Schematic of the crystal structure of Yb_3Pt_4, produced with the software of Ozawa and Kang (Ref. 20). The top figure shows an unusual projection, normal to a (10–30 9) plane, showing how the rhombohedral crystal structure can be seen in relation to a simple cubic structure. Structural octahedra (bottom), as explained in the text, depict Pt_6Pt [larger, lighter (red)] and Yb_6Pt [smaller, darker (blue)]. The relation between these structural octahedra and the simple cubic structure is shown as well.

Specific heat between 0.5 and 300 K, and magnetization at 4 K and in fields up to 14 T were measured in Quantum Design physical property measurement systems, respectively, equipped with a He-3 option and with a vibrating sample magnetometer option.

III. CRYSTAL AND MAGNETIC STRUCTURE

A. Crystal structure

Yb_3Pt_4 crystallizes[20] in the rhombohedral Pu_3Pd_4-type of structure, where Pu can be replaced by all rare earths except Eu, as well as by Y, and Pd by Pt.[16,21–23] Th_3Pd_4 (Ref. 22) and Zr_3Pd_4 (Ref. 24) have also been reported to form in this structure type. For the rare-earth compounds, no deviations from the lanthanide contraction have been observed,[16,22] indicating that both Ce and Yb are trivalent in these compounds.

Although YbPt forms in the FeB-type structure,[25] not in the layered cubic CsCl-type structure, we can describe the rhombohedral Yb_3Pt_4 structure in terms of this CsCl-type YbPt.[26] Figure 1 shows an unusual projection of the crystal structure of Yb_3Pt_4, viewed normal to a (10–30 9) plane. There are layers of Pt atoms and layers of Yb atoms. In these Yb layers, 1/7 of the atoms are replaced by Pt atoms in an ordered fashion. Besides this, the Yb_3Pt_4 structure is also distorted away from cubic symmetry, a distortion which also involves a shortening of the distances between the Yb-layer

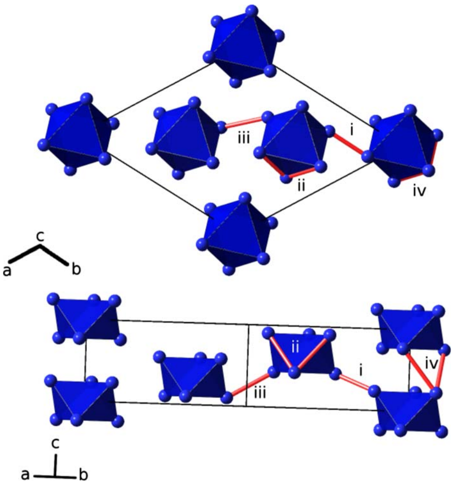

FIG. 2. (Color online) Schematic of structural Yb octahedra in the unit cell of Yb_3Pt_4, from two perspectives, emphasizing the Yb-Yb near-neighbor distances shorter than 4 Å, denoted as (i), (ii), (iii), and (iv). Every Yb atom has one (i) Yb nearest neighbor residing on a neighboring octahedron, at ~3.37 Å, and two next-nearest Yb neighbors (ii) on the same structural octahedron, at ~3.64 Å. Two pairs of farther-neighboring Yb atoms lie at (iii) ~3.80 Å and (iv) ~3.89 Å.

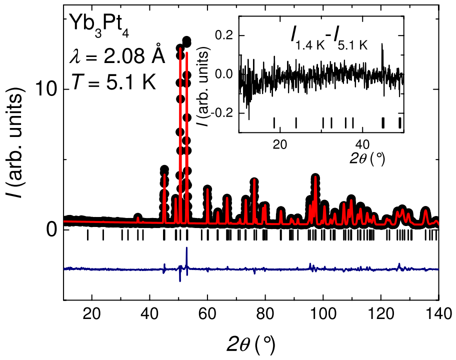

FIG. 3. (Color online) High-resolution neutron-powder-diffraction data (dots), Rietveld fit (line) and allowed Bragg reflections (tick marks) for Yb_3Pt_4, measured at 5.1 K. The lower trace is the difference between the data and the fit, on the same scale. The inset shows the difference between the 5.1 and 1.4 K data (line) indicating that the difference between these two is statistically insignificant even at the indicated Bragg reflections (tick marks).

Pt atoms and their surrounding Yb atoms.[24] This shortening allows us, for descriptive purposes, to divide the structure into two types of spatially separated octahedra with a Pt atom in the center. Of these, one type has Yb atoms at 18*f* on the corners surrounding the Pt atom at 2*a* and may be considered "Yb_6Pt" octahedra. The other type has Pt atoms at 18*f* surrounding the Pt atom at 2*b* and are thus "Pt_6Pt" octahedra. Note that these octahedra are not coordination polyhedra, which can be found in Refs. 7 and 21. In the top right part of Fig. 1 the structure is represented with these two types of octahedra. Viewed in this unusual way, the Yb_3Pt_4 crystal structure may be visualized as a stacking of layers of Yb_6Pt and Pt_6Pt octahedra. Note that the sides of the two different kinds of stacked octahedra are almost parallel.

The rhombohedral crystal structure of Yb_3Pt_4 can be represented by parallel chains of alternating Yb_6Pt and Pt_6Pt octahedra. The octahedra on neighboring chains are shifted with respect to one another. A rhombohedral unit cell consists of a stacked pair of these unequally sized, parallel-sided octahedra. A hexagonal unit cell, see Fig. 1 (bottom), consists of a stacked pair translated by (2/3,1/3,1/3) and by (1/3,2/3,2/3). Though parallel to one another, the sides of the Yb_6Pt and Pt_6Pt octahedra are not parallel to the crystal axes. Figure 2 shows a cross section of this hexagonal unit cell, showing the Yb-Yb distances which are shorter than 4 Å. Significantly, every Yb atom has only one Yb nearest neighbor, which greatly simplifies the magnetic structure, as we will see below.

B. High-resolution neutron-powder diffraction

We present in Fig. 3 a high-resolution neutron-powder-diffraction pattern which was measured at 5.1 K, i.e., in the paramagnetic phase. Rietveld analysis indicates that the diffraction pattern can be indexed according to the room-temperature space group $R\bar{3}$, with lattice parameters $a=12.8687(2)$ Å and $c=5.6160(1)$ Å. These lattice parameters are smaller than the room-temperature values $a=12.94$ Å and $c=5.655$ Å reported above, which can be ascribed to thermal contraction.

Further Rietveld refinement of the 5.1 K diffraction pattern fully conforms to the Pu_3Pd_4-type of structure as described in Sec. III A. The results of our best fit, which included background parameters, a scale factor, and peak shape parameters, are shown in Fig. 3 and are summarized in Table I. In accordance with detailed work on single crystals,[7] we found that variations in the site occupancies were insignificant, and therefore we fixed the sites to be fully occupied. The refined coordinates for the Yb 18*f* and the Pt 18*f* are

TABLE I. Refined structural parameters for Yb_3Pt_4 obtained from high-resolution neutron diffraction at 5.1 K. Space group $R\bar{3}$, $a=12.8687(2)$ Å, $c=5.6160(1)$ Å, $R_p=0.055$, $R_{wp}=0.072$, and $\chi^2=3.8$.

Atom (site)	x/a	y/b	z/c	Occ.	B_{iso} (Å)
Pt(3*a*)	0	0	0	1	0.28(5)
Pt(3*b*)	0	0	0.5	1	0.28(5)
Pt(18*f*)	0.2693(2)	0.2171(2)	0.2786(4)	1	0.28(5)
Yb(18*f*)	0.0421(2)	0.2111(1)	0.2335(3)	1	0.47(4)

very similar to the room-temperature values found by Palenzona and, in more detail, by Bennett *et al.*[7,16] Including isotropic thermal factors improved the fit. Our best fit was made with different thermal factors for the different species, Yb and Pt. Permitting the possibility of different thermal factors for the different Pt sites provided no further improvement to the fit. We also included a preferential-orientation parameter to improve our refinement, using a modified March function, as implemented by FULLPROF.[17] The modeled preferred-orientation vector was parallel to the *c* axis, and the refined parameter was found equal to 0.921(2), indicating a slight needlelike habit of the crystals. This is reasonable since the crystals that we coarsely ground for the powder typically were somewhat longer in the *c* direction than in the planar directions.

Having used the data taken at 5.1 K to verify the crystal structure of our powder sample, we next measured a neutron-powder-diffraction pattern at 1.4 K, i.e in the magnetically ordered phase below T_N=2.4 K. The inset of Fig. 3 shows the difference between the two diffraction patterns. This comparison did not reveal any magnetic intensity, finding that there is no statistically significant difference between the diffraction intensities obtained above and below T_N. A separate refinement of the low-temperature diffraction pattern established that there is no shift of the Bragg peak positions, and that the lattice parameters refined from the 5.1 and 1.4 K data were the same within 1×10^{-4}. As we will show in the next section, magnetic intensity was only observed when we sacrificed resolution in favor of scattered neutron intensity.

C. High-intensity neutron-powder diffraction

We successfully observed new magnetic intensity below T_N in high-intensity low-resolution powder-diffraction experiments. Figure 4 (top) compares diffraction patterns measured at 5 and 1.4 K, demonstrating that the (110) reflection is significantly more intense at 1.4 K than at 5 K. Figure 4 (bottom) shows the difference between patterns measured at 5 and 1.4 K. This difference pattern shows that at 1.4 K, there is new diffracted intensity at multiple Bragg-peak positions, making feasible the determination of the magnetic structure which is the major result we report here.

We confirm that this new intensity is related to the AF transition by a performing single-crystal neutron-diffraction experiment. Figure 5 shows the temperature-dependent intensity of the [110] reflection, measured by summing the counts of the centered BT9 detector, at temperatures between 1.4 and 4 K. The data were obtained over the course of multiple sweeps, with temperatures both increasing and decreasing. Starting at the lowest temperature, this [110] intensity decreases continuously, up to about 2.4 K, above which it remains constant. These results indicate a magnetic-ordering temperature of about 2.4 K, in excellent agreement with our previous results from specific heat, dc and ac magnetic susceptibilities, and electrical resistivities.[6,7] As was also the case in these earlier measurements, we observed neither thermal hysteresis nor a sudden change in this order parameter near T_N, suggesting that the ordering transition is continuous and well described by a mean-field expression.

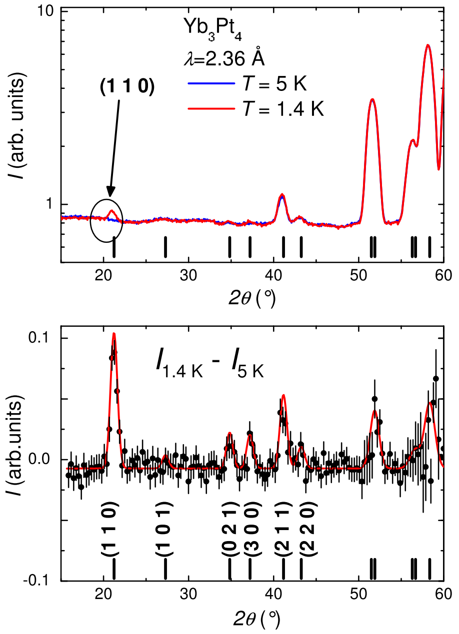

FIG. 4. (Color online) (Top) Low-resolution neutron-powder-diffraction patterns (log scale), measured at 5 and 1.4 K. The tick marks indicate Bragg positions. The lines connecting the data points are guides for the eye. The arrow indicates the strongest magnetic Bragg-peak position, (110). (Bottom) The difference between the neutron-powder-diffraction patterns at 5 and 1.4 K (linear scale). The (red) line is a profile-matched Rietveld fit, described in the text. Bragg-peak positions are indicated by tick marks. The indexed peaks were used for magnetic-structure refinement.

Furthermore, because the magnetic intensity in every case appears at Bragg-peak positions which have intensity above T_N, the magnetic unit cell is the same as the crystallographic unit cell. We note that this is also the case[10] for the magnetic structure of isostructural Yb$_3$Pd$_4$. Such a structure, with propagation vector $\boldsymbol{k}=0$, is often associated with ferromagnetism, but in this case, as we will see below, it is due to a $\boldsymbol{k}=0$ antiferromagnetic structure.

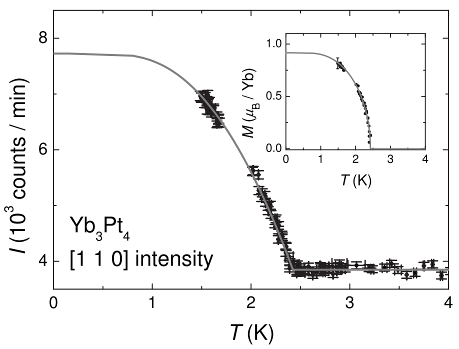

FIG. 5. The temperature-dependent intensity of the (110) nuclear and magnetic Bragg peak measured on a single crystal. The was line was calculated from the mean-field spin $\frac{1}{2}$ model with T_N=2.42(3) K. The inset shows the temperature-dependent ordered Yb moment, where the overall scale factor was determined from refined 1.4 K diffraction data as described in the text.

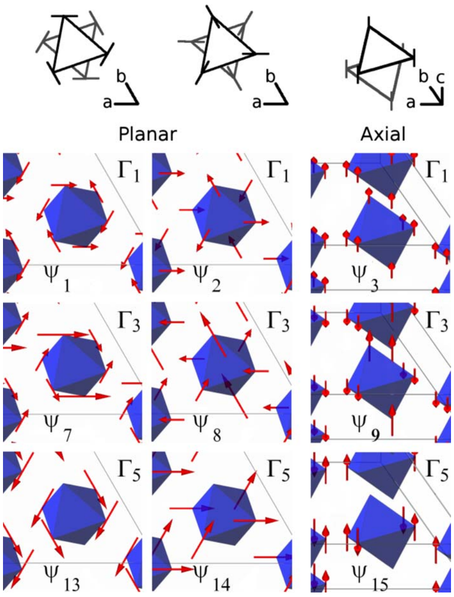

FIG. 6. (Color online) Basis vectors belonging to "ferromagnetic" IRs Γ1, Γ3, and Γ5, used to model the magnetic structures for Yb_3Pt_4.

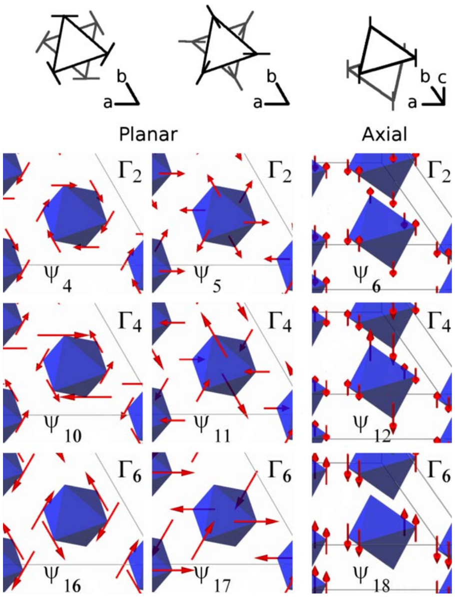

FIG. 7. (Color online) Basis vectors belonging to "antiferromagnetic" IRs Γ2, Γ4, and Γ6, used to model the magnetic structures for Yb_3Pt_4.

D. Representation analysis

We will test our diffraction data against magnetic-structure models obtained from representation analysis. These models are linear combinations, given by coefficients, of magnetic structure patterns, called basis vectors (BVs), for magnetic-moment carrying atoms. The choice of BVs to be included in a magnetic-structure model is limited and is wholly determined by symmetry. A number of BVs form an irreducible representation (IR) or a corepresentation (CR) of those space-group elements that leave the magnetic-propagation vector $\boldsymbol{k}$ invariant. If we apply Landau theory for continuous phase transitions then only one representation, an IR or a CR,[19,27] is involved in the magnetic order, and therefore the BVs belonging to a single representation. Since our magnetic-propagation vector $k=0$, we need to examine the BVs belonging to the IRs and CRs of the space group $R\bar{3}$ itself, for the magnetic Yb atoms on the Yb_6Pt octahedra. According to the program SARAH, there are six one-dimensional IRs, with three BVs each. Among these six IRs, there are two pairs of CRs,[19,28] namely, IRs Γ3 and Γ5, and Γ4 and Γ6, which means that these IRs, as well as their BVs, will be considered combined.

Each IR has two BVs that describe components of the magnetic structure in the plane perpendicular to the *c* axis (from here: planar) and one BV that describes a component of the magnetic structure parallel to the *c* axis (from here: axial). The IRs can be split in two parts, Γn $(n=1,3,5)$, and Γn $(n=2,4,6)$, respectively. For $n=1,3,5$ *some* BVs show a nonzero net magnetization and are ferromagnetic (F). For $n=2,4,6$ *all* BVs show no net magnetization and are antiferromagnetic. A schematic drawing of the 18 BVs is given in Fig. 6, for the IRs with (a) ferromagnetic BV(s), and Fig. 7, for the antiferromagnetic IRs, respectively. Every hexagonal unit cell contains three Yb_6Pt structural octahedra and on each of these the magnetic-moment configuration is the same. Therefore, we choose to display the BVs centered on a single Yb_6Pt octahedron, emphasizing the planar moments by viewing octahedra parallel to the *c* axis, and emphasizing the axial moments by viewing octahedra at an angle of ~30° from the *c* axis. In the figures, each row contains a different IR. In each, the third column contains the axial BVs while the first two columns contain the planar BVs. The IRs Γ_n can also be divided in three categories: two IRs $(n=1,2)$ with BVs that have equal moments on all Yb sites, two IRs $(n=3,4)$ with BVs that have 2/3 of the Yb moments half the size of the other 1/3, and two IRs $(n=5,6)$ with BVs that have nonzero size on 2/3 of the Yb moments and zero on the other 1/3.

A structural octahedron consists of two equilateral triangles with moments on each vertex. For the equal-moment configurations with the moments planar, these triangles carry AF structures where the moments on the vertices are aligned with the crystal axes and rotated by 120° with respect to one another. For the nonequal-moment configurations with the moments planar, these triangles form canted F structures. For the equal-moment configurations with axial moments, these triangles correspond to F structures but if the moments on each site are *not* equal then the structures on these triangles are AF. Pairs of IRs Γ1 and Γ2, Γ3 and Γ4, and Γ5 and Γ6, are analogous, as their respective BVs form pairs which are composed of the same triangular moieties described here. The difference between the BVs of the "F" and the "AF" IRs, is the direction of the moments on the top triangle relative to those on the bottom triangle, as can be appreciated by comparing, for example, BV $\psi 1$ $(\psi 2)$ to $\psi 4$ $(\psi 5)$.

Figures 6 and 7 show that the moments on individual Yb sites are rotated by 120° in the two planar BVs comprising an IR. However, it is not possible to rotate the crystal and at the same time obtain the other planar BV belonging to that

IR. We are therefore able to distinguish between different planar BVs for a given IR from a powder-diffraction experiment.[19,29] Another consequence is that the refined planar basis-vector coefficients have no linear correspondence with the size of the magnetic moment. We note further that the IRs which are part of a CR here each produce the same structure factors in our calculations and therefore Γ3(4) cannot be distinguished from Γ5(6). We will therefore only use IRs Γ3 and Γ4, as well as Γ1 and Γ2 for our refinements.

In a recent publication, Litvin[30] produced crystallographic tables of magnetic space groups. The magnetic space groups presented here are based on the so-called two-colored space groups and consequently only include equal-moment magnetic structures. Equal-moment IRs Γ1 and Γ2 are comparable to the magnetic space groups $R\bar{3}$ and $R\bar{3}'$, respectively. We note that models which can be constructed using the unequal-moment IRs Γ3-6 cannot be constructed from these magnetic space groups, requiring instead a more involved multicolored space-group analysis.[31]

E. Magnetic-structure refinement

The 1.4 K low-resolution diffraction pattern presented in Fig. 4(a) was used for a Le Bail-type[15] profile match, fitting for zero-offset, lattice parameters, background, and peak-shape parameters. For the refined lattice parameters we found $a=12.803(7)$ Å, and $c=5.602(4)$ Å, in agreement with values found in our high-resolution experiment described above. The agreement factors for this fit were $R_p=0.019$ and $R_{wp}=0.024$.

We determined a scale factor from the 5 K diffraction pattern of Fig. 4. For this, we use the profile-matched parameters found for the 1.4 K pattern, together with the atomic positions, thermal factors, as well as the preferred-orientation parameter, found from the refinement of the 5.1 K high-resolution data of Sec. III B. This yielded the scale factor with a refined estimated error of 0.4%. The agreement factors for this fit were $R_p=0.027$ and $R_{wp}=0.037$, which compares well to the values obtained from the profile matching above.

We determined the best fitting magnetic-structure model for each of the four IRs under consideration by refining the BV coefficients for the "magnetic-only" subtracted pattern of Fig. 4 (bottom) while we kept the scale parameter and the other parameters determined above (except the background parameters), fixed to the value determined on the full 1.4 and 5 K patterns. We included diffracted intensity only up to $2\theta=45°$, thus avoiding the relatively noisy background caused by the strong nuclear peaks at larger diffraction angles in Fig. 4(b). An initial Le Bail-type profile refinement yielded agreement factors of $R_p=0.0142$ and $R_{wp}=0.0177$. This can be considered the best possible fit since here the Bragg-intensities themselves are fit parameters and generated to best match the observed intensities.[15] The results of the refinements of the best-fitting magnetic structure models are shown in Fig. 8 and summarized in Table II. The overall best-fitting magnetic structure model is generated by the BVs of the AF IR Γ2 since that model gave *exactly* the same agreement factors as the model-free profile refinement. Second best is the AF best-fitting model described by the BVs of IR Γ4. Besides the slightly poorer fit for this Γ4 model than for the Γ2 model due to the unequal moments we may have expected structural deformations,[19] for which we have no evidence. The best-fitting model generated by F IRs Γ3 and Γ1 provides a significantly poorer description of the magnetic diffraction and it should be noted here that the refinement for Γ1 was not stable.

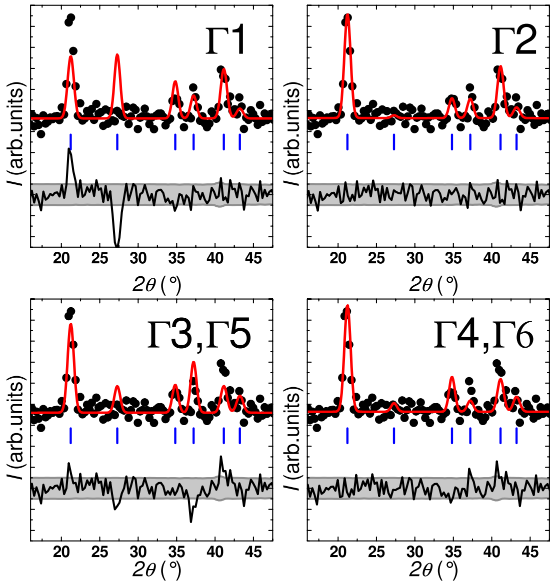

FIG. 8. (Color online) For each of the considered IRs (Γ1-4): magnetic-only diffraction pattern (dots) for Yb_3Pt_4 at 1.4 K, together with best fit (line) and difference pattern (line) on top of shaded error band estimated from data of Fig. 4.

Table II also includes the size of the ordered Yb magnetic moment for the best-fitting models. Averaged moments are given for the structures belonging to unequal-moment IRs Γ3

TABLE II. Magnetic refinement results for Yb_3Pt_4 at 1.4 K are tabulated for each of the considered IRs, with their BVs and their best-fit coefficients, as well as the average Yb moment μ and the agreement factors R_p and R_{wp} for each model. The best-fitting model has Γ2.

IR	BV	coefficient	μ (μ_B/Yb)	R_p	R_{wp}
Γ1	$\psi 1$	0.44(4)			
	$\psi 2$	0.36(2)			
	$\psi 3$	0.34(3)	0.89(9)	0.0233	0.0403
Γ2	$\psi 4$	0.38(1)			
	$\psi 5$	0.34(2)			
	$\psi 6$	0.18(2)	0.81(5)	0.0142	0.0177
Γ3	$\psi 7$	−0.11(4)			
	$\psi 8$	−0.23(2)			
	$\psi 9$	0.247(8)	1.6(2)	0.0168	0.0204
Γ4	$\psi 10$	0.14(2)			
	$\psi 11$	0.08(7)			
	$\psi 12$	0.228(5)	0.86(9)	0.0152	0.0189

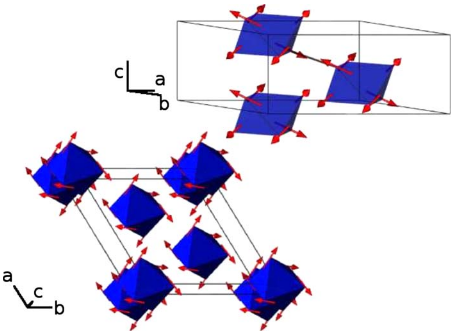

FIG. 9. (Color online) Two perspectives of a schematic view of the best refined magnetic-structure model for Yb_3Pt_4 at 1.4 K.

and Γ4. The average ordered moments for the four best-structure models due to Γ1, Γ2, and Γ4 are all close to $0.85\mu_B$ whereas the best-fitting model belonging to IR Γ3 has an average moment of $1.6\mu_B/\mathrm{Yb}$. The ordered moment for the best-fitting structure is about $0.81(5)\mu_B/\mathrm{Yb}$ at 1.4 K. This value was used, together with the temperature-dependent intensity of the single-crystal [110] reflection, to normalize the order parameter, which is displayed in the inset of Fig. 5.

Finally, we refined the scale factor for the full 1.4 K diffraction pattern, including also the best-fitting magnetic structure model according to IR Γ2. Within error, we found the same scale factor as the one we used for the magnetic structure refinement, with agreement factors of $R_p=0.025$ and $R_{wp}=0.036$, comparable to the agreement factors found for the 5 K data, as described above.

A schematic of the proposed magnetic structure for Yb_3Pt_4 is presented in Fig. 9. In this structure, the ordered Yb moments are all of the same size and have both planar and axial components. Yb octahedra form the basic building block of the extended magnetic structure. In our model all Yb moments point outward from such an octahedron, where the Yb moments on the top triangle point upward, and the moments on the bottom triangle point downward. The directions of the moments are such that the moments on two nearest-neighbor Yb ions, residing in neighboring Yb octahedra, point almost exactly toward each other, see Fig. 9. As calculated from Table II, the planar component of the ordered moment is $0.73\mu_B$, while the axial component is $0.34\mu_B$, thus the ordered moments make an angle of 64° with the c axis.

IV. CRYSTAL FIELD AND EXCHANGE ANISOTROPY

A central goal of our magnetic-structure determination was to gain insight into whether the Yb moments should be considered spatially localized in zero field or not. In this section, we seek to rationalize the magnitude of the moment deduced from our diffraction experiments within a crystal-field model, including both the crystal field and exchange anisotropies. In the triclinic environment of the Yb ions in Yb_3Pt_4, the crystal-electric field (CEF) lifts the $2J+1$ (=eightfold) degeneracy of the magnetic $4f$ shell into four doublets, causing the single-ion CEF anisotropy. As stated previously, specific-heat measurements provided evidence for this crystal-field splitting. We present in Fig. 10 an improved analysis of the magnetic contribution to specific heat C_M, obtained by subtracting the Lu_3Pt_4 (Ref. 32) specific heat from the measured Yb_3Pt_4 specific heat $C(T)$. The ordering peak at $T_N=2.4$ K (Ref. 7) is prominent and looks similar to an included ideal mean-field $S=1/2$ specific-heat peak[33,34] but it reaches only about 80% of the theoretical value at T_N. The entropy associated with magnetic order is very similar as in the earlier measurement, approaching the doublet value of $R \ln 2$ only at ~10 K. We note that, in agreement with our earlier report, the Sommerfeld coefficient $\gamma=C/T$ in the ordered state is very small, certainly no larger than 10 $\mathrm{mJ/mol\,K^2}$ at $T=0$ K. Also clear is a broad Schottky-type peak with a maximum near 75 K. This peak was fit above 10 K with a Schottky-type expression accounting for the ground-state doublet and three excited doublets. The line in Fig. 10 shows the quality of the fit with these excited doublets at energies of 7.1 (5), 20 (2), and 30 (6) meV. These values are notably different from values found by Bennett *et al.*,[7] who found 4.3 and 10.9 meV, which we mainly ascribe to fact that they used a Debye expression to account for the lattice contribution of specific heat, where we used Lu_3Pt_4 data.

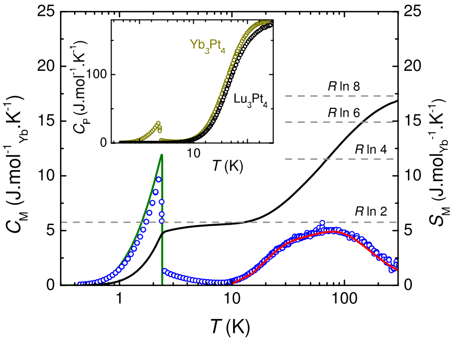

FIG. 10. (Color online) The difference (open circles) between the measured specific heats of Yb_3Pt_4 and Lu_3Pt_4, C_M, and its associated entropy S (solid black line). The line (green) below 2.4 K is an idealized mean-field spin $\frac{1}{2}$ specific-heat peak with T_N =2.4 K. The fit line (red) above 10 K is a fit to a Schottky expression, yielding excited doublets at 7.1, 20, and 30 meV. For comparison, the inset shows the specific heat of both Yb_3Pt_4 (dark yellow) and Lu_3Pt_4 (black).

Inelastic neutron-scattering measurements provide an independent determination of the zero-field CEF splitting and the results are shown in Fig. 11. We see that there are four sharp peaks, occurring at 7.5, 21, 30, and 34 meV. We believe that the 34 meV peak is a spurious scattering effect[35] and that the other three excitations correspond to transitions among the CEF-split doublets. While we do not present the data here, the wave vector dependence of the intensity of these peaks agrees qualitatively with the Yb^{3+} magnetic form factor while their excitation energies do not vary. What is more, the values of the excitation energies found in the inelastic neutron-scattering experiment are in excellent agreement with those found from the specific heat. We conclude that the antiferromagnetic order in Yb_3Pt_4 involves a doublet state which is well separated from the higher lying states.

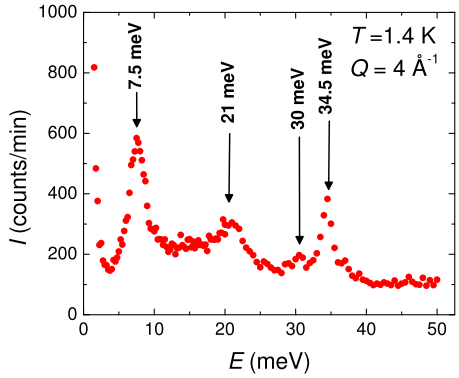

FIG. 11. (Color online) Inelastic neutron-scattering spectrum of 7 g of Yb_3Pt_4 powder, recorded at 1.4 K with a wave vector of 4 Å^{-1}. Excited states are found at 7.5, 21, and 30 meV. The sharp peak at 34.5 meV is likely spurious.

The general success of the CEF scenario and the relatively large magnitude of the Yb moments found in the neutron-diffraction measurements are consistent with a description in which the Yb moment is localized and not significantly itinerant. No significant difference was observed in these excitations as we pass into the antiferromagnetic state. In principle, we might expect that the exchange interaction would split the ground doublet and mix these states with higher lying states. However, our energy resolution is not sufficient in this experiment to resolve this effect since this splitting should be comparable to T_N=2.4 K, ~0.21 meV.

A more practical way to extract information about the relative roles of the exchange- and crystal-field anisotropies is from the analysis of the isothermal magnetization. $M(H)$ is shown in Fig. 12 for T=4 K and for fields as large as 14 T applied both parallel and perpendicular to the c axis. In both cases, the magnetization is nonlinear and resembles a Brillouin function. The magnetization for $H \perp c$ axis saturates above ~8 T and the saturation moment is estimated to be $2.12\mu_B/$Yb, by extrapolating the magnetization measured between 8 and 14 T to zero field, denoted by a dashed gray line in Fig. 12. The magnetization for $H \| c$ axis is lower in all fields, approaching saturation above ~10 T. The saturation moment obtained from extrapolation is $\sim 0.57\mu_B/$Yb for this field direction. We use the model that was given by Bonville *et al.*[36] to describe these magnetization data. This molecular-field model, which is solved self-consistently, assumes that the measured magnetization is generated by the splitting of a well-separated Yb^{3+} doublet ground state in an external field, and includes anisotropic g factors, as well as anisotropic molecular exchange-interaction parameters λ, and van Vleck-type terms ϵ to describe the magnetization which ensues due to the quantum-mechanical mixing of the ground-state doublet with the excited doublets. The best fit generated from this model is compared to the $H \perp c$ axis $M(H)$ curve in Fig. 12. We see that the agreement is excellent and indicates that g=4.23, λ=0.053 T/μ_B, and $\epsilon = 2.35 \times 10^{-2}$ μ_B/T for fields in the ab plane. In the absence of a Van Vleck-like term, this g factor would lead to a saturation magnetization of $2.12\mu_B/$Yb, in excellent agreement with the zero-field value obtained by extrapolation. Since the molecular field parameter λ for $H \perp c$ axis is weakly positive, we conclude that exchange interactions in the plane are weak and ferromagnetic. The analysis is less satisfactory for axial fields $H \| c$ axis. A free-parameter fit [lower (red) line] for the magnetization with H axial gives g=1.44, λ=1.40 T/μ_B, and $\epsilon = 4.12 \times 10^{-2}$ μ_B/T. In the absence of a Van Vleck-type term, this g factor would lead to a saturation magnetization of $0.72\mu_B/$Yb, in poor agreement with the zero-field value of $0.57\mu_B/$Yb obtained by extrapolation. In fact, it was not possible to extract a unique set of model parameters from $M(H)$ for $H \| c$ axis so we cannot comment quantitatively on the anisotropy in the g factors and the molecular exchange λ. Nonetheless, our analysis of the magnetization suggests that the CEF-induced magnetic anisotropy strongly favors the crystallographic plane, and from the weak molecular exchange found in the ab plane, we conclude that the ordering exchange is anisotropic and favors the c axis. We note here, that similar, though less conclusive, ideas were presented to describe the magnetic structure of isostructural Yb_3Pd_4.[10]

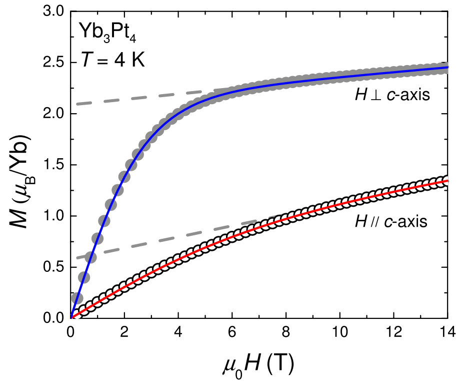

FIG. 12. (Color online) Magnetization of Yb_3Pt_4 measured at 4 K for fields $H \perp c$ axis (closed symbols) and for $H \| c$ axis (open symbols). The upper (blue) line is a fit for $H \perp c$ axis while the lower (red) line is the fit for $H \| c$ axis, as described in the text. The gray lines are extrapolations of the high field magnetization to zero field.

V. CONCLUSIONS

We confirm by neutron-powder-diffraction experiments that the intermetallic compound Yb_3Pt_4 is antiferromagnetic. The zero-field magnetic structure has the same unit cell as the crystal structure so the propagation vector $\boldsymbol{k}$=0. The order parameter, determined from the temperature dependence of a single-crystal [110] reflection, confirms the magnetic-ordering temperature at T_N=2.4 K, and indicates that the magnetic-ordering transition is continuous and mean-fieldlike. A proposed model for the zero-field magnetic structure was determined using representation analysis. The fundamental building blocks of this magnetic structure are Yb octahedra, with triads of moments oriented at 120° in the ab plane, half with a component along the c axis and half in the opposite direction. Because $\boldsymbol{k}$=0, there is no net moment within the octahedron. Individual Yb moments are oriented toward their nearest neighbors, which lie in different octahedra. Consequently, the moments have both axial and planar components.

Like the magnetic-order parameter, the temperature dependence of the specific heat $C(T)$, displays a mean-fieldlike transition near T_N=2.4 K. The specific-heat step $\Delta C(T_N)$ amounts to only ~80% of the value expected for an effective-S=1/2 moment. It is possible that this reduced anomaly results from a substantial degree of hybridization between the Yb moments and the conduction electrons, although there are no other indications of this hybridization, such as an incipient Kondo effect or any enhancement of the Sommerfeld coefficient γ, which is found to be less than 10 mJ/mol K^2 in the ordered state of Yb_3Pt_4.[6]

A primary motivation for our experiments was to determine whether the Yb moments can be considered spatially localized, such as those reported for Ce in the isostructural Ce compound Ce_3Pt_4,[9] or are significantly itinerant. Neutron-diffraction measurements assign an ordered state moment of $0.81\mu_B$ to each Yb ion at 1.4 K, which is strongly suggestive that a localized-moment description is more suitable. In agreement, specific-heat and inelastic neutron-scattering measurements concur that the moments which order antiferromagnetically belong to a well-separated doublet ground state, signaling that the degeneracy of Yb^{3+} is fully lifted in the low-symmetry crystal electric fields experienced by the Yb ions in Yb_3Pt_4. Our analysis of the anisotropic field-dependent magnetization $M(T)$ rationalizes the magnetically ordered structure. Here, the crystal electric field seeks to keep the moments in the magnetically easy *ab* plane, while a molecular exchange field is, with a small transverse component, almost parallel to the hard *c* axis. These interactions can together be held responsible for the canting of the Yb moments out of the easy *ab* plane as well as for the size of the ordered moment. The overall success of this crystal field plus exchange model is a strong indication that the Yb moments can be considered to be spatially localized and that the *f* electrons are excluded from the Fermi surface, at least in zero field.

ACKNOWLEDGMENTS

We are indebted to A. S. Wills, A. Kreyssig, P. Stephens, A. Moodenbaugh, W. Ratcliff, and P. Khalifah for valuable discussions and for help with experiments. Work at the Brookhaven National Laboratory was supported by the U.S. Department of Energy, Office of Basic Energy Sciences. Work at Stony Brook University was supported by the National Science Foundation under Grant No. NSF-DMR-0405961. We acknowledge the support of the National Institute of Standards and Technology, U.S. Department of Commerce, in providing the neutron research facilities used in this work.

---

*yjanssen@bnl.gov

[1] H. v. Löhneysen, A. Rosch, M. Vojta, and P. Wölfle, Rev. Mod. Phys. **79**, 1015 (2007).
[2] G. R. Stewart, Rev. Mod. Phys. **73**, 797 (2001).
[3] G. R. Stewart, Rev. Mod. Phys. **78**, 743 (2006).
[4] P. Gegenwart, Q. Si, and F. Steglich, Nat. Phys. **4**, 186 (2008).
[5] S. Nakatsuji, K. Kuga, Y. Machida, T. Tayama, T. Sakakibara, Y. Karaki, H. Ishimoto, S. Yonezawa, Y. Maeno, E. Pearson, G. G. Lonzarich, L. Balicas, H. Lee, and Z. Fisk, Nat. Phys. **4**, 603 (2008).
[6] M. C. Bennett, D. A. Sokolov, M. S. Kim, Y. Janssen, Y. Yiu, W. J. Gannon, and M. C. Aronson, arXiv:0812.1082 (unpublished).
[7] M. Bennett, P. Khalifah, D. Sokolov, W. Gannon, Y. Yiu, M. Kim, C. Henderson, and M. Aronson, J. Magn. Magn. Mater. **321**, 2021 (2009).
[8] H. Gamari-Seale and J. K. Yakinthos, J. Appl. Phys. **50**, 2315 (1979).
[9] G. F. von Blanckenhagen and G. R. Stewart, Solid State Commun. **108**, 535 (1998).
[10] P. Bonville, J. A. Hodges, P. Imbert, G. Jéhanno, and P. Thuéry, J. Magn. Magn. Mater. **136**, 238 (1994).
[11] Z. Fisk and J. P. Remeika, in *Handbook on the Physics and Chemistry of Rare Earths*, edited by K. A. Gschneidner, Jr. and L. Eyring (North-Holland, Amsterdam, 1989), Vol. 12.
[12] P. C. Canfield and Z. Fisk, Philos. Mag. B **65**, 1117 (1992).
[13] P. C. Canfield and I. R. Fisher, J. Cryst. Growth **225**, 155 (2001).
[14] B. Hunter, Lhpm-rietica, www.rietica.org
[15] A. Le Bail, H. Duroy, and J. L. Fourquet, Mater. Res. Bull. **23**, 447 (1988).
[16] A. Palenzona, J. Less-Common Met. **53**, 133 (1977).
[17] T. Roisnel and J. Rodríguez-Carvajal, Mater. Sci. Forum **378-381**, 118 (2001).
[18] A. S. Wills, Physica B **276-278**, 280 (2000).
[19] A. S. Wills (unpublished).
[20] T. C. Ozawa and S. J. Kang, J. Appl. Crystallogr. **37**, 679 (2004).
[21] D. T. Cromer, A. C. Larson, and R. B. Roof, Jr., Acta Crystallogr., Sect. B: Struct. Crystallogr. Cryst. Chem. **29**, 564 (1973).
[22] A. Palenzona and A. Iandelli, J. Less-Common Met. **34**, 121 (1974).
[23] A. Iandelli and A. Palenzona, J. Less-Common Met. **43**, 205 (1975).
[24] L. A. Bendersky, J. K. Stalick, and R. M. Waterstrat, J. Alloys Compd. **201**, 121 (1993).
[25] Q. Johnson, R. G. Bedford, and E. Catalano, J. Less-Common Met. **24**, 335 (1971).
[26] K. Cenzual, J. L. Jorda, and E. Parthé, Acta Crystallogr., Sect. C: Cryst. Struct. Commun. **44**, 14 (1988).
[27] P. G. Radaelli and L. C. Chapon, Phys. Rev. B **76**, 054428 (2007).
[28] M. Tinkham, *Group Theory and Quantum Mechanics* (Dover, Mineola, NY, 1992).
[29] G. Shirane, Acta Crystallogr. **12**, 282 (1959).
[30] D. B. Litvin, Acta Crystallogr., Sect. A: Found. Crystallogr. **64**, 419 (2008).
[31] D. Harker, Acta Crystallogr., Sect. A: Found. Crystallogr. **37**, 286 (1981).
[32] Sample was obtained by alloying constituent elements in an Ar-atmosphere arc melting furnace.

[33] H. R. Ott, L. D. Woolf, M. B. Maple, and D. C. Johnston, J. Low Temp. Phys. **39**, 383 (1980).

[34] H. R. Ott, G. Keller, W. Odoni, L. D. Woolf, M. B. Maple, D. C. Johnston, and H. A. Mook, Phys. Rev. B **25**, 477 (1982).

[35] G. Shirane, S. M. Shapiro, and J. M. Tranquada, *Neutron Scattering with a Triple-Axis Spectrometer: Basic Techniques* (Cambridge University Press, Cambridge, UK, 2002).

[36] P. Bonville, P. Bellot, J. A. Hodges, P. Imbert, G. Jéhanno, G. Le Bras, J. Hammann, L. Leylekian, G. Chevrier, P. Thuéry, L. D'Onofrio, A. Hamzic, and A. Barthélémy, Physica B **182**, 105 (1992).